# PLAXIS

CONNECT Edition V22.00

## User Defined Soil Models - NorSand: An elasto-plastic model for soil behaviour with static liquefaction

Bentley®
*Advancing* Infrastructure

Last Updated: January 14, 2022

# Table of Contents


**Chapter 1: Introduction ..... 3**

1.1 General concepts ..... 4
1.2 Mathematical Notation ..... 5

**Chapter 2: Model Formulation ..... 7**

2.1 Operating friction ratio Mi ..... 10
2.2 Softening parameter S ..... 11
2.3 Soil state measurements ..... 12

**Chapter 3: Model Parameters ..... 14**

3.1 Critical state locus: parameters Γ, λe or Ca, Cb and Cc ..... 14
3.2 Dilation limit: parameter χtc ..... 14
3.3 Strength parameter: Mtc and N ..... 15
3.4 Plastic hardening: parameter Ho and HΨ ..... 15
3.5 Elasticity: properties G100, nG and ν ..... 15
3.6 Typical Values ..... 16

**Chapter 4: Model performance and numerical validation ..... 20**

4.1 Model Performance ..... 20
4.2 Numerical validation ..... 24

**Chapter 5: UDSM implementation in PLAXIS finite element code ..... 27**

5.1 Material Parameters ..... 27
5.2 State variables ..... 29

**Chapter 6: Finite Element Analyses ..... 31**

**Chapter 7: References ..... 35**

# 1 Introduction

NorSand (NS) is a critical state soil model within the wider theory of work-hardening plasticity. Critical State Soil Mechanics (CSSM) applies across the spectrum of soil types and states, from soft clays through to dense sands. Originating in work by the US Army Corp of Engineers for Franklin Falls dam (Lyman, 1938 (on page 35)), their canonical relation of the critical state to soil behaviour combines with the Taylor-Bishop strength model (Bishop, 1950 (on page 35)), using the stability postulate (Drucker, 1951 (on page 35)), to give a general framework with the particular attribute of computing the effect of void ratio on soil behaviour from fundamental principles. NorSand (NS) is a strict implementation of CSSM, using the state parameter (the difference between the void ratio and its critical value at the current stress, Figure 1 (on page 3)) as a key controlling variable.

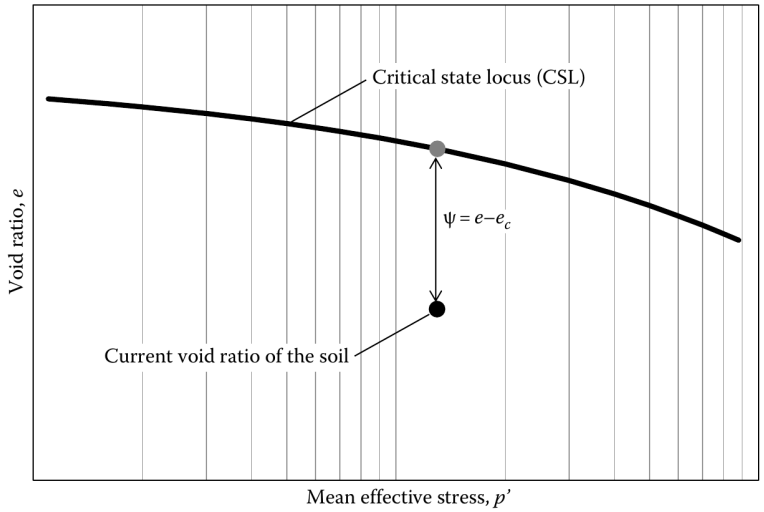


*Figure 1: Definition of state parameter ψ, and over-consolidation ratio R (figure after Jefferies, 2016).*

The "Sand'' in the NS name is only there to emphasize NS ability to properly represent dilation found with dense soils, although the most prominent use of the model has been to simulate static liquefaction of loose silts (e.g., Fundao Dam, Morgenstern et al, 2016; Cadia Dam, Morgenstern et al, 2019; and Brumadinho Dam, Robertson et al, 2020). Soil properties in NS are mostly standard in the geotechnical community and do not vary with void ratio or confining stress. All properties are defined under triaxial compression (as conventional in geotechnical laboratory testing). In principle, a minimum of three triaxial compression tests are required; practically, a few more are needed to give precision and redundancy.

NS is a state model, and thus requires the initial/in situ state parameter to be defined as an input; most users will derive this input from CPT data but other methods can be used. The inputs of the model specifying the initial states are denoted through the subscript *o* to emphasize that they are initial values specified by the user. NS is an effective stress model, computing undrained behaviour and offering also options as to how soil behaviour is represented, in particular the form of the operating zero-dilation friction ratio and the nature of the critical state

locus. This NS implementation is for standard monotonic loading, drained or undrained, with a particular focus on static liquefaction. Specifically, this release is consistent with the version of NS given in *Appendix C* of Jefferies and Been (2016) (on page 35) with minor updates for improved computational performance.

## 1.1 General concepts

Before detailing the proposed implementation of the model, some general concepts related to the elasto-plastic theory are recalled hereafter:

- The strain is additively split in the elastic and plastic components, respectively:

$$\varepsilon_{ij}^{t} = \varepsilon_{ij}^{el} + \varepsilon_{ij}^{pl}.$$

- The stress $\sigma_{ij}$ is computed with isotropic elasticity:

$$\sigma_{ij} = C_{ijkl}\varepsilon_{kl}^{el}.$$

- The yield surface $f$ is used to define the elastic domain and admissibility of the stress state.
- The plastic flow of the model is prescribed through a flow rule:

$$\dot{\varepsilon}_{ij}^{pl} = \Lambda\left(\frac{\partial g}{\partial \sigma_{ij}}\right)$$

where $g$ represents the plastic potential function and prescribes the direction of the plastic flow. $\Lambda$ stands for the plastic multiplier which allows one to calculate the amount of plastic strain.

- A similar equation is also defined to govern the evolution of the variable $\Gamma_i$ of the model: $\Gamma_i = \Lambda h_i$, where $h_i$ is the hardening vector of the model.
- The state of the material is governed by the so-called *Khun-Tucker hardening conditions*:

$$f(\sigma_{ij}, \Gamma_k) \leq 0, \quad \Lambda f(\sigma_{ij}, \Gamma_k) = 0, \quad \Lambda \geq 0$$

if $f < 0$ then the material state is elastic (i.e., $\Lambda = 0$), otherwise $f = 0$ means that the state of the material can be in plastic or neutral loading (i.e., $\Lambda = 0$ corresponds to neutral loading while $\Lambda > 0$ is the condition for plastic loading). Plastic or neutral loading can be determined by considering further conditions, the so-called *persistency conditions*:

$$\dot{f}(\sigma_{ij}, \Gamma_k) \leq 0, \quad \Lambda \dot{f}(\sigma_{ij}, \Gamma_k) = 0, \quad \Lambda \geq 0$$

where

| | | |
|---|---|---|
| $\dot{f} < 0$ | = | Elastic unloading. |
| $\dot{f} = 0, \Lambda > 0$ | = | Plastic loading. |
| $\dot{f} = 0, \Lambda = 0$ | = | Neutral loading. |

## 1.2 Mathematical Notation

It is common practice in geomechanical modeling to express the stress dependency of the yield and plastic potential surfaces as a function of stress invariants, i.e., the mean stress $p$, the stress deviator $q$ and the Lode's angle $\theta$. They are defined as:

$$\begin{cases} p = \dfrac{tr(\sigma)}{3} = \dfrac{\sigma_{ij}\delta_{ij}}{3} = \dfrac{\sigma_{xx} + \sigma_{yy} + \sigma_{yy}}{3} \\ q = \sqrt{\dfrac{3}{2}(s_{ij}s_{ij})} = \sqrt{\dfrac{3}{2}}\|s\| \\ \theta = \dfrac{1}{3}\arcsin\left[\sqrt{6}\left(\dfrac{tr(s^3)}{tr(s^2)^{3/2}}\right)\right] \end{cases}$$

where $s_{ij}$ is the deviator component of the stress state (i.e., $s_{ij} = \sigma_{ij} - p{\cdot}\delta_{ij}$ , $\delta_{ij}$ is Kronecker's symbol) and the trace $tr(\cdot)$ gives the sum of the diagonal terms of the matrix (i.e., $\mathrm{tr}(\sigma_{ij}) = \sigma_{xx} + \sigma_{yy} + \sigma_{zz} = 3P$).

A general representation of the stress deviator and its norm is reported as:

$$s_{ij} = \begin{bmatrix} \sigma_{xx} - p & \sigma_{xy} & \sigma_{xz} \\ \sigma_{yx} & \sigma_{yy} - p & \sigma_{yz} \\ \sigma_{zx} & \sigma_{zy} & \sigma_{zz} - p \end{bmatrix}$$

$$\|s\| = \sqrt{(\sigma_{xx} - p)^2 + (\sigma_{yy} - p)^2 + (\sigma_{zz} - p)^2 + 2\left(\sigma_{xy}^2 + \sigma_{zy}^2 + \sigma_{zx}^2\right)}$$

Analogously, similar quantities are defined also for the strain tensor $\varepsilon_{ij}$:

$$\begin{cases} \varepsilon_v = \varepsilon_{xx} + \varepsilon_{yy} + \varepsilon_{zz} \\ \varepsilon_q = \sqrt{\dfrac{2}{3}\left(\varepsilon_{s_{ij}}\varepsilon_{s_{ij}}\right)} = \sqrt{\dfrac{2}{3}}\|\varepsilon_s\| \end{cases}$$

where $\varepsilon_v$ represents the volumetric strain, $\varepsilon_{s_{ij}}$ is the strain deviator which is defined as: $\varepsilon_{s_{ij}} = \varepsilon_{ij} - (\varepsilon_v \cdot \delta_{ij}) / 3$ .

$$\varepsilon_{s_{ij}} = \begin{bmatrix} \varepsilon_{xx} - \varepsilon_v/3 & \varepsilon_{xy} & \varepsilon_{xz} \\ \varepsilon_{yx} & \varepsilon_{yy} - \varepsilon_v/3 & \varepsilon_{yz} \\ \varepsilon_{zx} & \varepsilon_{zy} & \varepsilon_{zz} - \varepsilon_v/3 \end{bmatrix}$$

$$\|\varepsilon_s\| = \sqrt{\left(\varepsilon_{xx} - \frac{\varepsilon_v}{3}\right)^2 + \left(\varepsilon_{yy} - \frac{\varepsilon_v}{3}\right)^2 + \left(\varepsilon_{zz} - \frac{\varepsilon_v}{3}\right)^2 + 2\left(\varepsilon_{xy}^2 + \varepsilon_{zy}^2 + \varepsilon_{zx}^2\right)}$$

For triaxial stress paths ($\sigma_{xx} = \sigma_{yy} < \sigma_{zz}$, $\sigma_{xz} = \sigma_{xy} = \sigma_{yz} = 0$), the general definition of invariants can be simplified as:

$$p = (\sigma_{zz} + 2\sigma_{xx})/3 \qquad q = |\sigma_{zz} - \sigma_{xx}|$$

$$\varepsilon_v = (\varepsilon_{zz} + 2\varepsilon_{xx})/3 \qquad \varepsilon_q = 2|\varepsilon_{zz} - \varepsilon_{xx}|/3$$

In this context, the deviatoric and volumetric plastic strain are computed as:

$$D_p = \frac{\partial g}{\partial p} \Big/ \frac{\partial g}{\partial q} \qquad \begin{cases} \dot{\varepsilon}_v^p = \Lambda\left(\frac{\partial g}{\partial p}\right) \\ \dot{\varepsilon}_v^p = \Lambda\left(\frac{\partial g}{\partial q}\right) \end{cases}$$

where $D_p$ represents the so-called dilatancy function.

Hereafter, a positive compression convention will be adopted in accordance with the usual soil mechanics framework. All stress measures are considered as *effective* and, for the sake simplicity, the superscript ', commonly used in soil mechanics notation, will be omitted.

# 2 Model Formulation

Like other work-hardening plasticity models, NS is characterized by: pressure dependent elasticity, a yield surface, a plastic flow-rule and a hardening law. A central feature of NS is that it is based on a work dissipation postulate, which is a generalized formulation of the Taylor-Bishop strength mode (Bishop, 1950 (on page 35)), thus requiring that the stress and strain measures must be '*work conjugate*' for all stress combinations. For this purpose, the invariants introduced by Resende and Martin (1985) (on page 35) are adopted in the model formulation. While the stress invariants $p$ and $q$ are those that are standard in plasticity theory (and used in other PLAXIS models) the matching invariants of strain increments $\dot{\varepsilon}_v^p$ and $\dot{\varepsilon}_q^p$ are less familiar. NS uses the simple postulate that plastic work is only dissipated in distortion resulting to one form of stress-dilatancy which is the fundamental flow-rule adopted. This is largely the same as Original Cam Clay (Schofield and Wroth, 1968 (on page 35)), the difference being that NS allows the dissipation parameter (the zero-dilatancy '*frictional dissipation*' stress ratio $M_i$) to vary with soil state under control of the soil property $N$ rather than being just a function of the stress ratio $M_{tc}$ which corresponds to critical state friction (Figure 2 (on page 8)). The third stress invariant, the Lode angle $\theta$, does no work and is thus unconstrained by the work dissipation postulate other than the particular symmetries of triaxial compression and extension; the effect of $\theta$ is represented by an empirical modifying function for the flow-rule based on data from plane strain tests in sand (Conforth, 1961 (on page 35)).

NS also adopts Drucker's stability postulate such that the work-conjugate plastic strain increment vector is always normal to the yield surface in the $p$-$q$ plane. The basic NS yield surface is derived by using the adopted normality and the work-dissipation postulate, with the yield surface scaled by the '*image*' stress $p_{im}$ which is the stress state when $D_p=0$ (this is sometimes called the '*pseudo steady state*' or the '*phase-change*'). The requirement to limit dilation, in accordance with state-dilatancy (i.e., $D_p < \chi_{tc}\Psi = D_p^{min}$ ) is met by limiting the yield surface hardening such that $p_{im} < p_{mx}$ with $p_{mx}$ defined as a function of the miminum dilatancy; correspondingly, the hardening law has the form of a first-order rate equation, but with an evolving target. This gives NS a form of double-hardening where the yield surface evolves quickly to its current limiting size (conceptually associated with the formation of particle contacts) and tracks the evolution of this hardening limit which depends entirely on the state parameter. Thus, the yield surface can be established under any stress regime with the evolution to the critical state arising under distortional strain for increasing value of the stress ratio $\eta=q/p$; loading paths of constant or decreasing $\eta$ are '*consolidation*' without the soil tending to its critical state. Because the yield surface is decoupled from the critical state locus (CSL), an additional soil property is needed to describe the rate at which the yield surface responds to distortional strain: the hardening modulus, $H$. The corollary of this decoupling is that the CSL can have whatever form is needed to represent a soil, the only restriction being that the CSL must be a monotonic decreasing function of mean stress to be physically reasonable. Two popular forms of the CSL are implemented and they are reported here below with the entire set of constitutive equations defining NS model:

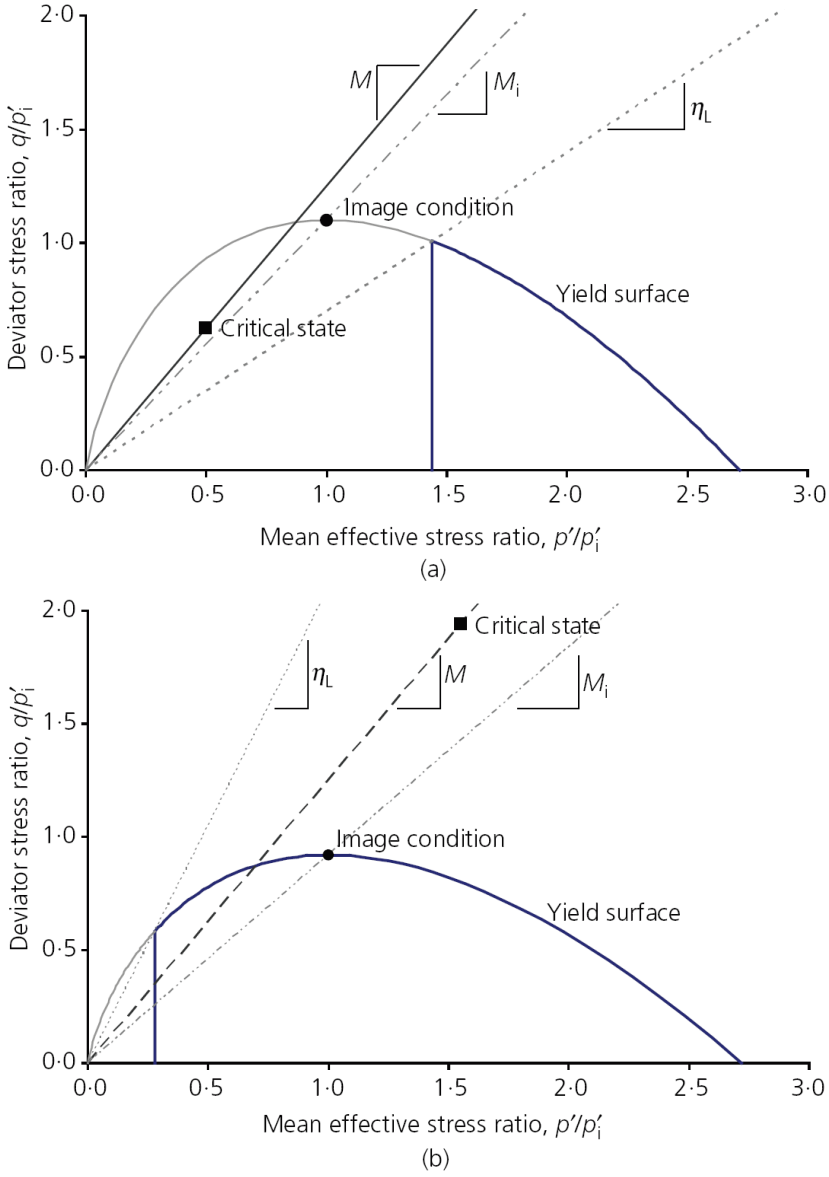


*Figure 2: llustration of the yield surface and limiting stress ratios for (a) very loose sands and (b) very dense sands (Figure after Jefferies, 2015)*

- Yield Surface:

$$f = q - \eta p \quad with \quad \eta = M_i\left[1 + \ln\left(\frac{p_{im}}{p}\right)\right] \qquad Eq.\ [1]$$

- Flow rule:

$$\frac{\dot{\varepsilon}_3^p}{\dot{\varepsilon}_1^p} = z_{3,tc} - (z_{3,tc} - z_{3,te})\cos\left(\frac{3\theta}{2} + \frac{\pi}{4}\right) \qquad \begin{cases} z_{3,tc} = \dfrac{2D_{tc}^p - 3}{2D_{tc}^p + 6}; & D_{tc}^p = D^p\left(\dfrac{M_{i,tc}}{M_i}\right) \\ z_{3,te} = \dfrac{2D_{te}^p + 6}{2D_{te}^p - 3}; & D_{te}^p = D^p\left(\dfrac{M_{i,te}}{M_i}\right) \end{cases} \qquad \textit{Eq. [2]}$$

$$\frac{\dot{\varepsilon}_2^p}{\dot{\varepsilon}_1^p} = \frac{aD^p - 1 + \dfrac{d\varepsilon_3}{d\varepsilon_1}(cD^p - 1)}{1 - bD^p} \qquad \begin{cases} a(\theta) = (\sin(\theta) + \sqrt{3}\cos(\theta))/3 \\ b(\theta) = -2\sin(\theta)/3 \\ c(\theta) = (\sin(\theta) - \sqrt{3}\cos(\theta))/3 \end{cases}$$

  where the dilatancy function $D^P$ is defined as $D^P = M_i - \eta$.

- Critical state locus:

$$\begin{aligned} &\textit{Option (a)} \quad e_c = \Gamma - \lambda \ln(p) \\ &\textit{Option (b)} \quad e_c = C_a - C_b\left(\frac{p}{p_{ref}}\right)^{C_c} \end{aligned} \qquad \textit{with} \qquad \begin{cases} \Psi = e - e_c(p) \\ \Psi_i = e - e_c(p_{im}) \end{cases} \qquad \textit{Eq. [3]}$$

- Hardening:

$$\dot{p}_{im} = \left[H\frac{p}{p_{im}}\frac{M_i}{M_{i,tc}}(p_{mx} - p_{im}) - S_{soft}\right]\dot{\varepsilon}_q^p \qquad p_{mx} = p\exp\left(-\frac{x_{tc}}{M_{i,tc}}\Psi\right) \qquad \textit{Eq. [4]}$$

It is worth remarking that the flow rule expressed as a function of the ratio of plastic strain increments (Eq. [2]) can be recast through a gradient of the plastic potential, consistently with an elasto-plastic framework. By employing the invariants introduced by Resende and Martin (1985) (on page 35) and the normality rule used to calculate the deviatoric plastic strain increment (i.e., $\dot{\varepsilon}_q^p = \Lambda\left(\partial f / \partial q\right) = \Lambda$), the plastic flow is rewritten as:

$$\begin{bmatrix} \dot{\varepsilon}_1^p \\ \dot{\varepsilon}_2^p \\ \dot{\varepsilon}_3^p \end{bmatrix} = \begin{bmatrix} \dot{\varepsilon}_q^p\left(\dfrac{q + pD^p}{\sigma_1 + z_2\sigma_2 + z_3\sigma_3}\right) \\ z_2\dot{\varepsilon}_1^p \\ z_3\dot{\varepsilon}_1^p \end{bmatrix} = \Lambda\begin{bmatrix} \dfrac{\partial g}{\partial \sigma_1} \\ z_2\dfrac{\partial g}{\partial \sigma_1} \\ z_3\dfrac{\partial g}{\partial \sigma_1} \end{bmatrix} = \Lambda\begin{bmatrix} \dfrac{\partial g}{\partial \sigma_1} \\ \dfrac{\partial g}{\partial \sigma_2} \\ \dfrac{\partial g}{\partial \sigma_3} \end{bmatrix} \qquad \textit{Eq. [5]}$$

Soil elasticity usually shows a dependence of both bulk and shear moduli on mean effective stress (i.e., *K* and *G*, respectively), as well as some dependence on void ratio. A constant Poisson's ratio is adopted to relate *G* and *K* to avoid unconservative elastic idealization. The shear modulus *G* is defined through a power-law expression which uses an exponent $n_G$ to further characterize soil behaviour. No effect of void ratio on *G* and *K* is included in this PLAXIS release of NS as such effects are generally minor within any defined soil stratum:

- Elasticity:

$$\begin{aligned} G &= G_{ref}\left(\frac{p}{p_{ref}}\right)^{nG} \\ K &= 2G\left(\frac{1+\nu}{3-6\nu}\right) \end{aligned} \qquad \textit{Eq. [6]}$$

## 2.1 Operating friction ratio $M_i$

Two options are offered for the zero-dilatancy friction ratio $M_i$ (Figure 3 (on page 10)), which are both based on the idea suggested by Li and Dafalias (2000) (on page 35) that $M_i$ should depend on Ψ.

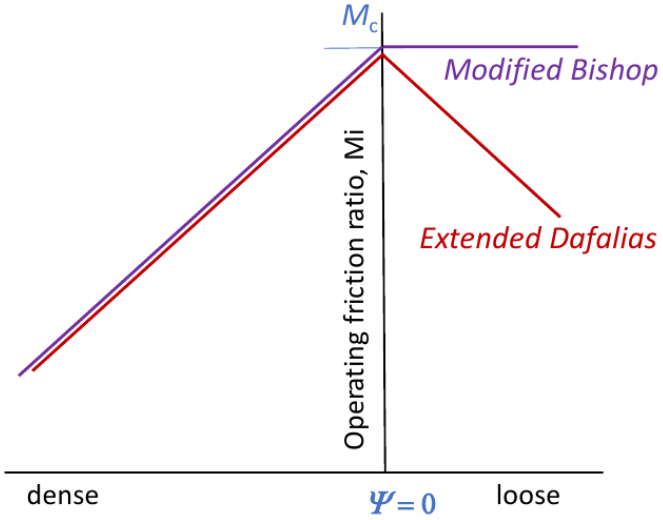


*Figure 3: Formulation of friction ratio $M_i$ according to Li and Dafalias (2000) and Bishop (1950)*

$M_i$ requires a two-stage evaluation: at first, the critical state friction ratio $M_c$ computed as a function of Lode angle $\theta$ (Jefferies and Shuttle, 2011 (on page 35)):

$$M_c = M(\theta) = M_{tc}\left[1 - \frac{M_{tc}}{3 + M_{tc}}\cos\left(\frac{3\theta}{2} + \frac{\pi}{4}\right)\right] \qquad Eq.\ [7]$$

with $M_c=M_{tc}$ in case of triaxial compression (i.e., $\theta= \pi/6$) and $M_c=3M_{tc}/(M_{tc}+3)$ in case of triaxial extension (i.e., $\theta=-\pi/6$). An intermediate step is required because if the critical friction ratio is expressed as a function of Ψ then neutral loading will cause the yield surface to change size (which is inadmissible) since $p$ varies during neutral loading, thus resulting to a change of Ψ. For this reason, the state parameter at a particular point on the yield surface is used (so it does not vary during neutral loading) and which is, conveniently, the image condition:

$$\Psi_i = e - CSL\ (p_{im}) \qquad Eq.\ [8]$$

where *CSL* is the chosen representation of the *CSL()* that gives $e_c$ (i.e., Option (a) or (b) reported in Eq. [3]).

A matching mapping of the soil dilatancy must also be used with Ψi, and which is:

$$X_i = \frac{X_{tc}}{1 - \lambda X_{tc}/M_{tc}} \qquad Eq.\ [9]$$

At last, this $M_c$ is now changed to an "*operating*" value $M_i$. As dense soils closely follow Nova's flowrule, NS always uses the following equation for the operating value $M_i$:

$$\Psi < 0 \rightarrow M_i = M\left(1 + \frac{N X_i}{M_{tc}}\Psi_i\right) \qquad Eq.\ [10]$$

The situation in loose soils is less clear, with some soils showing less ability to dissipate plastic work as they get progressively looser while others seem to more closely follow the *Taylor-Bishop* framework of a constant dissipation rate regardless how loose; both these frameworks are offered as options and the user can choose the one which best fits the soil being modeled. The two options are:

- Option A: *Taylor-Bishop*

$$\Psi \geq 0 \rightarrow M_i = M(\theta) \qquad Eq.\ [11]$$

- Option B: *Extended Dafalias*

$$\Psi \geq 0 \rightarrow M_i = M(\theta)\left(1 - \frac{N X_i}{M_{tc}}\Psi_i\right) \qquad Eq.\ [12]$$

If Ψ=0, NS yield surface intersects the *CSL* and $M_i$=$M_c$, consistently with the basic idealization of CSSM. Although taking $M_{tc}$ as a constant soil property is the dominant view in the literature, some test data suggests that very loose void ratios may reduce $M_{tc}$ (see Figure 16 of Been et al (1991) (on page 35)). Reduced $M_{tc}$, if present, will be most evident in soil states showing static liquefaction with large brittleness. The user can choose the proposed options (i.e., Option A or B) based on laboratory test data and switch between the two options according to the sign of $M_{tc}$: *Extended Dafalias* correspond to $M_{tc}$>*0*, while *Taylor-Bishop* is selected with $M_{tc}$<*0*.

## 2.2 Softening parameter *S*

The hardening limit of the yield surface $p_{mx}$ depends on $p$ as well as the soil's properties and void ratio. At variance with drained loading, for which the evolution of $p_{mi}$ is governed by the smooth change enforced through the first-order hardening law during undrained loading, the rate of change of $p$ can easily become faster than the basic hardening law, thus leading to $p_{mi} > p_{mx}$ (contrary to the basic principle of the hardening limit). For this reason, a softening term $S_{soft}$ is added to the hardening law resulting to a further decrease of the image stress $p_{mi}$ during undrained conditions (i.e., for drained loading $S_{soft} \equiv 0$). As a matter of fact, NS is derived from the CSSM axioms with the exception of this term $S_{soft}$. For this reason, whether to use $S_{soft}$ or not is a choice for the user:

$$D^p \leq 0 \rightarrow S_{soft} = S = 0$$
$$D^p > 0 \rightarrow S_{soft} = S \cdot \omega\left(\frac{\eta}{M_i}\right)\left(\frac{K}{p}\right) D^p p_{im} \qquad \omega = 1 - \lambda\frac{X_{tc}}{M_{tc}} \qquad S = 1 \qquad Eq.\ [13]$$

The possibility to add this further contribution in the softening response can be activated by the user through the flag S listed in the graphical interface (see section UDSM implementation in PLAXIS finite element code (on page 27)). NS does achieve the critical state with S = 0 (which is the "pure" version of the theory) with a rate less rapid than usually encountered in triaxial tests showing static liquefaction. Figure 4 (on page 12) illustrates the performance of NS for a very loose soil according to the selected value of the flag *S*.

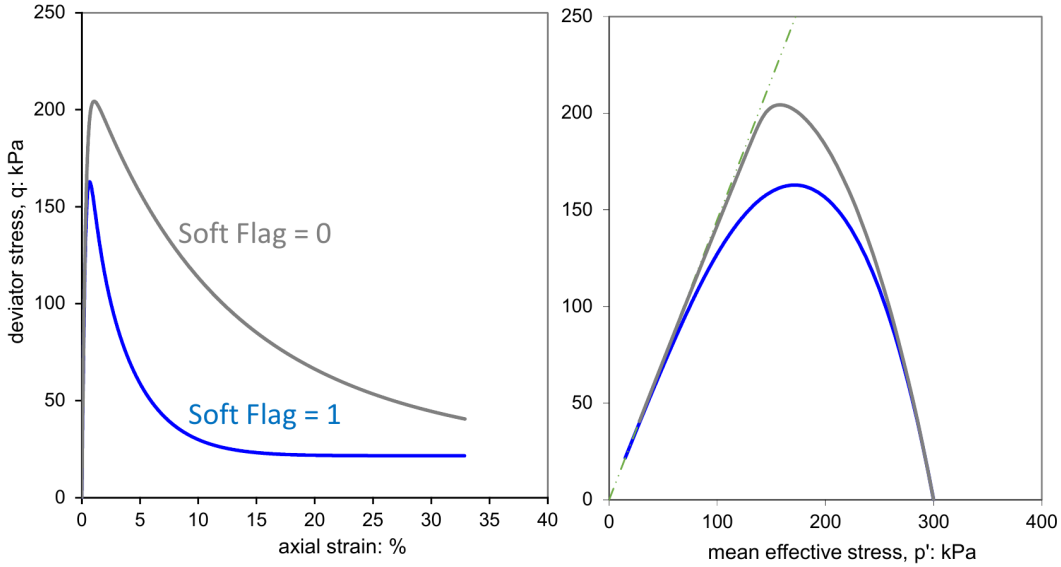


*Figure 4: Mechanical behaviour during an undrained triaxial test using the softening flag S=1.*

## 2.3 Soil state measurements

NS requires three *state* measures to specify the starting point for the calculations.

1. ***The geostatic stress state***: It is assigned using a single value of $K_o$; this is equivalent to assume a "*green field*" level-ground site as the starting point for any boundary value problem. In the case of constructed works, this is reasonable for the individual layers of soil placed, with the evolution of the stresses computed as further layers are placed. In the case of natural ground, ideally there should be a self-bored pressuremeter data through which evaluate the geostatic stress state. The geostatic stress-state gives initial values for $p_o$ and $q_o$, and thus $\eta_o$. These are then used to compute the normally consolidated yield surface image stress as:

$$p_{im}^{NC} = p_o \exp\left(\frac{\eta_o}{M_i} - 1\right) \qquad Eq.\ [14]$$

   The geostatic stress state depends on more than over-consolidation ratio, and the familiar $K_o = 1 - sin(\phi)$ is rarely a good representation. However, if there are no further information to determine $K_o$, the user can adopt $K_o$=0.7 as initial value which for loose or normally-consolidated soils can be considered a reasonable approximation.

2. ***The initial overconsolidation***: Overconsolidation pushes the yield surface away from the current stress-state thus:

$$p_{im,o} = R \cdot p_{im}^{NC} \qquad Eq.\ [15]$$

   where $R \geq 1$ is the input over-consolidation ratio. It is worth noting that what is reported as heavily overconsolidated (i.e., soils characterized by $R>>1$) is actually more accurately viewed as a dense soil. Thus, if modelling heavily over-consolidated deposits, it is suggested to use a dense choice for $\Psi_0$ combined with more modest estimate of $R$ to determine the initial position of the yield surface. The user can further verify

the effect of the overconsolidation by using the *Soil Test* facility in PLAXIS to better understand how these choices can affect the stress-strain response of the soil during the calibration process.

3. ***The state parameter*** $\Psi_o$ : The initial value of the state parameter it is assigned using a single value for each stratum. Although it is common to use void ratio as the ``input'' state variable for CSSM, the use of initial void ratio requires a precise knowledge of the CSL due to the key-role of the state parameter in controlling soil behaviour (not the void ratio itself). The problem therein is that natural variation in soil gradation within a single stratum results in a range of CSL's. However, it is found that common depositional conditions for the soil produces the same soil state parameter despite the natural changes in gradation - in essence, both void ratio and the CSL change together. This shows up in CPT soundings which profiles commonly show near constant values of $\Psi$ within identifiable strata. For this reason, $\Psi$ becomes the basic input for boundary value problems using CSSM.

   In the case of existing grounds, it is assumed to have CPT data as the starting point of a numerical modeling. In the case of new works, the state parameter must be estimated for the fill and it will be usual to base those estimates on prior experience which has been tested using the CPT. If just modelling laboratory tests (i.e., to confirm a calibration) the state parameter is calculated from the measured void ratio and fitted CSL. The state parameter will show natural variability and the assigned $\Psi_o$ should be "characteristic" in the sense of the structural eurocode (i.e., EN1997); choosing $\Psi_o$ such that about 80-90 % of the stratum is more dilatant is often appropriate (see Chapter 5 of Jefferies & Been, 2016 (on page 35)).

# 3 Model Parameters

NS soil parameters are independent of void ratio and confining stress, and thus constant for any soil. It is often helpful to optimize the value of these parameters through a calibration process in which laboratory experiments are considered to simulate the soil behavior at different conditions. The soil properties are all defined/measured under triaxial compression; NS contains the mapping of these triaxially determined properties to general stress states. All parameters are dimensionless other than: *i)* the two alternative parameters $\Gamma$ or $C_a$ of the CSL model that have an implicit stress-level of 1 kPa and 0 kPa, respectively; and, *ii)* the reference elastic shear modulus $G_{100}$ that has units of stress. With the only exception of the hardening modulus, most of the NS parameters are conventionally known/understood and are readily found simply by appropriate plotting of test data. An accurate description of the calibration process can be found in Chapter 9 of Jefferies & Been (2016) (on page 35) which gives more details about this procedure. It is a good practice to formally model every test, drained and undrained, to validate the inferred soil properties. In doing this, the precision in the laboratory for measurement of initial test conditions is about $\Delta\Psi = \pm 0.02$, so allowing some small changes in the reported initial conditions is both allowable and often helps to understand the soil properties.

## 3.1 Critical state locus: parameters $\Gamma$, $\lambda_e$ or $C_a$, $C_b$ and $C_c$

Two options for the critical state void ratio $e_c$ are presently offered, one being the conventional semi-log form and the other a power-law that is becoming widely used (Eq. [3]). It is worth noting that care is needed to avoid choosing void ratios above the CSL when modelling undrained loading with the power-law CSL, as the specified state may imply zero critical state strength and thus cause numerical instability. The CSL can be determined reliably, but particular laboratory procedures ("End of Test Freezing") are required; Reid et al (2020) document achievable reliability, with laboratory procedures described in Appendix B of Jefferies & Been (2016) (on page 35). CSSM derivations lead to natural logarithms, but conventional representation of laboratory data is to use base 10; care is needed when specifying the semi-log CSL. The two properties are simply related with $\lambda_e = \lambda_{10}/2.3$.

## 3.2 Dilation limit: parameter $\chi_{tc}$

NS limits dilation using a first-order rate approach; this is equivalent to what some refer to as the Hvorslev surface. Because of the compression-positive convention,"maximum'' dilation is $D^p_{min}$, and it is defined under triaxial compression. The dilation limit is given by:

$$D^p_{min} = \chi_{tc}\Psi \qquad Eq.\ [16]$$

The soil property $\chi_{tc}$ is determined by carrying out dense drained tests and then plotting the measured dilatancy limit versus the state parameter at that limit (i.e., not the initial state parameter of the test). Although this parameter affects loose soils behaviour, it is difficult to separate from other properties influencing loose soil behaviour and which prevents direct determination from simple plotting. Thus, even if the focus of interest is loose soil some tests on dense samples are helpful. However, silts can be challenging with present laboratory procedures sometimes being unable to produce dense samples of some silts; in this situation $\chi_{tc}$ has to be inferred from modelling loose soils by iteratively adjusting $\chi_{tc}$ to best-fit the test data after all other properties have been determined.

## 3.3 Strength parameter: $M_{tc}$ and $N$

Although CSSM models generally only incorporate the critical friction ratio, test data does not support this view in detail. For this reason, NS uses Nova's extension with a second parameter $N$ has been introduced:

$$\eta_{\max} = M_{tc} - 1(1 - N)D_{min}^{p} \quad (under\ triaxial\ conditions) \qquad Eq.\ [17]$$

The usual method to determine $M_{tc}$ and $N$ is the Bishop's method, in which $D_{min}^{p}$ and $\eta_{max}$ data from a set of drained triaxial tests on dense soil are plotted to calibrate $M_{tc}$ and $N$, being those parameters the best trend line fitting the experimental data (see Figure 6 (on page 18) and Figure 7 (on page 18) ). It is possible to estimate $M_{tc}$ directly from tests on loose soils drained or undrained, since that is the end-point of their stress-paths. In this case, caution is needed because: *i)* the conversion of measured load to calculated axial stress depends on the "*area ratio correction*", which correction may not be a good representation of how the sample deformed; and, *ii)* in the case of undrained tests the mean effective stress depends on the difference between the measurements of two transducers and accuracy may be much degraded. If no dense tests are available, $N \approx 0.3$ is a plausible initial estimate (it is a value that commonly arises in reported data).

## 3.4 Plastic hardening: parameter $H_o$ and $H_\Psi$

Plastic hardening modulus is the only NS-specific property as it relates only to the NS hardening law. These properties $H_o$ and $H_\Psi$ are dimensionless and both are needed because most soils show a dependence of hardening on the state parameter. There is also an element of softening associated with increasing $\eta$, and better fits are obtained to test data if that is recognized. Thus, the following is used for the hardening modulus:

$$H = H_o - H_\Psi \Psi \qquad Eq.\ [18]$$

It is suggested to, first fitting/calibrating NS to a soil just by setting $H_\Psi$=0 and varying $H_o$ until the trend for $H$ with $\Psi$ becomes clear. An element of Original Cam Clay, with its use as $1/(\lambda-\kappa)$ as the plastic hardening modulus, carries over to NS and a good starting point is usually $H_o = 2/\lambda$. Both $H_o$ and $H_\Psi$ are determined by optimizing a set of drained triaxial tests which include loose and dense states.

## 3.5 Elasticity: properties $G_{100}$, $n_G$ and $\nu$

NS anchors elasticity to $G_{ref} \equiv G_{100}$, which is the value of the mean effective stress at the reference pressure $p_{ref}$ equal to 100 kPa (a widespread convention), combined with an exponent $n_G$ for a power-law trend, thus introducing the stress-dependency on this modulus. To avoid issues with non-conservative elasticity, a constant Poisson's ratio $\nu$ is used to compute the elastic bulk modulus $K$ from $G$. Thus, elasticity is:

$$G = G_{ref}\left(\frac{p}{p_{ref}}\right)^{n_G}, \quad K = \frac{2}{3}\left(\frac{1+\nu}{1-2\nu}\right)G \qquad Eq.\ [19]$$

Geophysical measurements, whether in situ (seismic CPT or seismic dilatometer) or in the laboratory ("bender elements''), have come to dominate geotechnical engineering and thus the elastic shear modulus is now the basic elastic input. However, there is an effect of confining stress-level on the modulus in most cases. The elastic model used assumes that a set of geophysical measurements have been reduced to this two-property model, that allows a single parameter set to be used in a soil stratum as opposed to having to model the soil in thinner layers each with its own $G$. Commonly, $\nu$ is not measured and 0.2 is adopted as "not unreasonable'' based on the extensive testing of Ticino sand.

## 3.6 Typical Values

Soil mechanical properties are influenced by grain shape, grain mineralogy, and particle size distribution among other factors. However, the effects of these geological measures on mechanical properties remain imprecise although different soil type provides a basis for a classification of the corresponding parameters. An example is presented in Table 1 (on page 16) where NS parameters are calibrated by soil type.

**Table 1: Examples of NS parameters by soil type**

| **Soil: *Natural Sands*** | $\lambda_{10}$ | $M_{tc}$ | **N** | $\chi_{tc}$ | **H** |
|---|---|---|---|---|---|
| Erksak ($D_{50}$=330 $\mu$ m) | 0.050 | 1.23 | 0.30 | 4.5 | 100-650 $\psi$ |
| Nerlerk ($D_{50}$=270 $\mu$ m) | 0.045 | 1.26 | 0.35 | 4.1 | 85-75 $\psi$ |
| Ticino ($D_{50}$=530 $\mu$ m) | 0.055 | 1.27 | 0.33 | 4.0 | 55-850$\psi$ |
| Ottawa ($D_{50}$=530 $\mu$ m) | 0.028 | 1.13 | 0.25 | 4.7 | 130-1400$\psi$ |
| Fraser River ($D_{50}$=270 $\mu$ m) | 0.080 | 1.46 | 0.50 | 3.2 | 95-400$\psi$ |
| **Soil: *Natural Silts*** | $\lambda_{10}$ | $M_{tc}$ | **N** | $\chi_{tc}$ | **H** |
| John Hart | 0.18 | 1.31 | 0.3 | 2.5 | 50 |
| Coquitlam | 0.2 | 1.2 | 0.3 | 2.0 | 45 |

| Soil: *Tailing Silts* | $\lambda_{10}$ | $M_{tc}$ | $N$ | $\chi_{tc}$ | $H$ |
|---|---|---|---|---|---|
| EKO | 0.480 | 1.37 | 0.00 | 0.8 | 30 |
| FKX | 0.550 | 1.26 | 0.40 | 2.5 | 17-100$\psi$ |
| NCS | 0.246 | 1.35 | 0.30 | 2.5 | 20-100$\psi$ |
| NCP | 0.175 | 1.40 | 0.30 | 2.5 | 30-200$\psi$ |
| RCR | 0.159 | 1.25 | 0.30 | 4.0 | 25 |
| TC1 | 0.105 | 1.51 | 0.35 | 7.7 | 73-500$\psi$ |

The CSL remains the least clearly controlled behaviour by geological measures. In Figure 5 (on page 17) a selection of CSL's for various soils, from sands to clays, is presented. As can be seen, the semi-log representation of the CSL is a reasonable approximation for at least a one-order of magnitude range in mean pressure and this adequacy is independent of soil type. Analyses involving a wider range of confining stress may require the power-law representation of the CSL. The "altitude" of the CSL (i.e., properties $\Gamma$ or $C_a$) are unrelated to geological classification of soil type, but there is a trend to greater compressibility (the properties $\lambda$ or $C_b$) as the soil becomes finer; however, well-graded soils can be much stiffer than their fines content might first indicate. It is useful to best-fit a semi-log CSL to soil data over the range 40 – 400 kPa even though a power-law CSL may be needed for a better precision; the values quoted in Table 1 (on page 16) are based on this and show the range of soil properties for different type of soils.

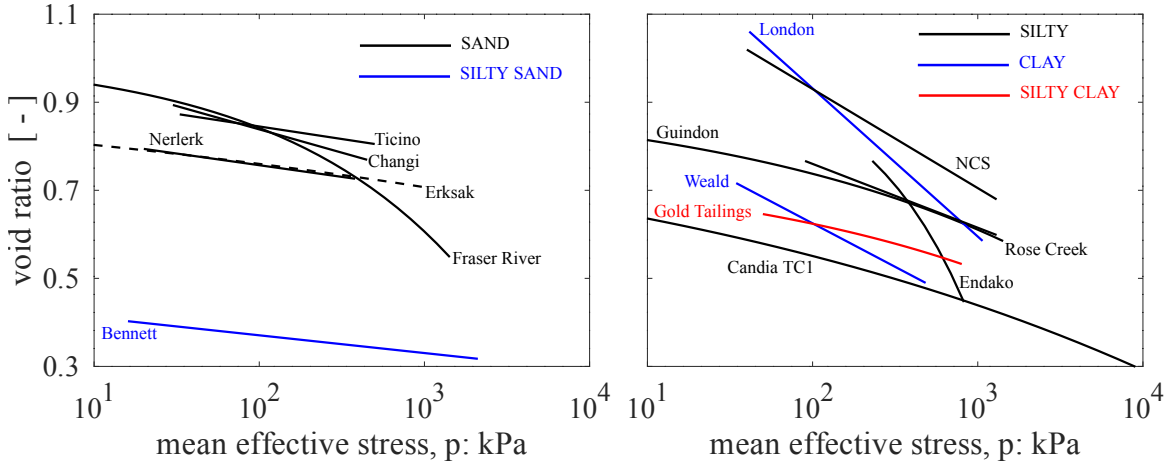


*Figure 5: CSLs for different soils: (a) sands and silty sands, (b) silties, clays and silty clays (data after Jefferies, 2020).*

The critical friction ratio (i.e., property $M_{tc}$) of sandier soils is much influenced by grain shape, with this effect well illustrated by Cho et al. (2006) (on page 35) who provides a useful database. Tailings, being normally crushed materials with angular particles, often have markedly greater friction than natural soils. Equally, there is often an effect of void ratio with very loose soils showing reduced $M_{tc}$ compared to that in a compact to dense state (see Figure 16 of Been et al. (1991) (on page 35)). There has been little systematic investigation of the influence of geological measures on the volumetric coupling (i.e., the parameter $N$), with experience in regard to this property largely confined to sands with less than 15% fines; $N$≈0.3 appears to be appropriate for many soils. The state-dilatancy property (i.e., the parameter $\chi_{tc}$) captures the tendency with which particles can move past each other as the soil deforms and appears to be markedly influenced by the particle size distribution with a further effect from mineralogy of the soil particles. In Figure 6 (on page 18) and Figure 7 (on page 18), a data

set available for different type of soils is used to calibrate $\eta_{max}$ and $D_{min}^{p}$ as reported in Jefferies (2020) (on page 35).

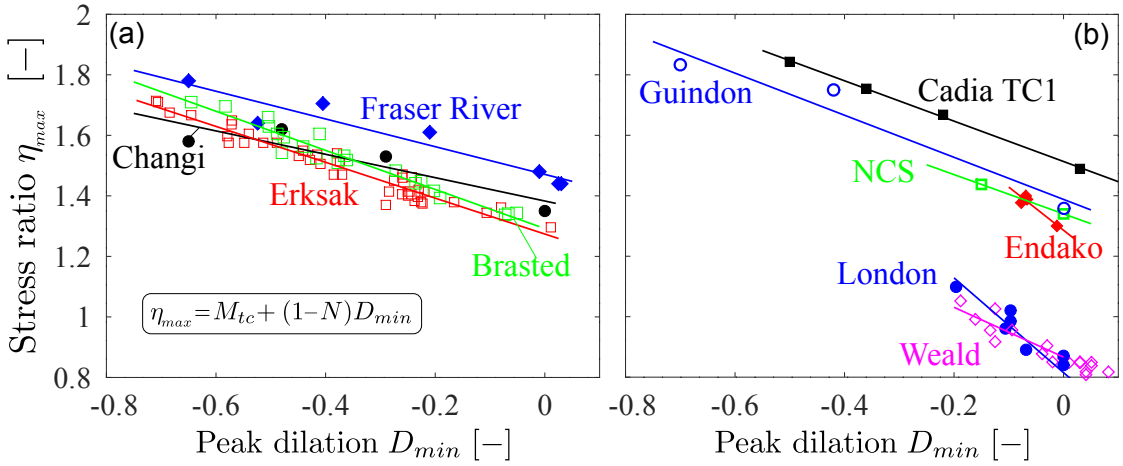


*Figure 6: CSLs for different soils: (a) sands and silty sands, (b) silties, clays and silty clays (data after Jefferies, 2020)*

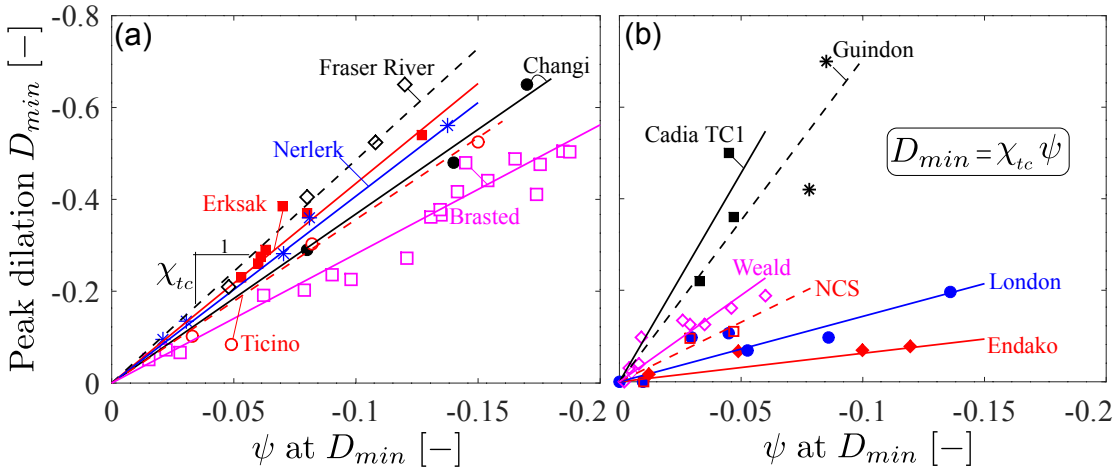


*Figure 7: CSLs for different soils: (a) sands and silty sands, (b) silties, clays and silty clays (data after Jefferies, 2020)*

The hardening modulus $H$ appears markedly correlated to $1/\lambda$, with compressible soils having smaller values of $H$. Although not general for most type of soils which are calibrated with a constant modulus, there appears a dependence of $H$ on $\Psi$ which can be captured by calibrating the parameter $H_\Psi$. Elasticity is much affected by stress level, commonly to a power-law with an exponent on stress in the range $0.4 < n_G < 0.8$; when expressed as a shear rigidity, $I_r$ (i.e., a dimensionless quantity defined as $G_{max}/p'$), a wide range is encountered because of this effect of stress level. There is also an effect of void ratio and a lesser effect of aging. It is standard practice to measure the elastic shear modulus using geophysical methods, either vertical seismic profiling (often using a *seismic cone*) or with *bender elements* in the laboratory; it is common to reduce these geophysically measured values to fit undrained tests depending on soft flag (the reduction is often by a factor of 3 for *S=1*). Poisson's ratio is usually taken in the range $0.15 < \nu < 0.25$ without measurements other than validation by fitting the stress-paths measured in undrained triaxial tests.

A typical range of values characterizing the parameters of NS model to simulate sand behaviour is presented in Table 2 (on page 19) according to the values proposed in Jefferies and Been (2016) (on page 35).

**Table 2: Model parameters employed in the material point computations presented in Figures. 8-13**

| $I_r$ | $\nu$ | $\Gamma$ | $\lambda_e$ | $M_{tc}$ | $N$ | $\chi_{tc}$ | $H$ |
|---|---|---|---|---|---|---|---|
| 100-600 | 0.1-0.3 | 0.9-1.4 | 0.01-0.07 | 1.2-1.5 | 0.2-0.5 | 2-5 | 25-500 |

It is worth nothing that, as remarked in Jefferies and Been (2016) (on page 35) (see Appendix H), the mechanical response calculated with NorSand model can replicate the constitutive behaviour of Original Cam Clay (OCC) by selecting the following set of parameters: $N = 0,\ \ H = 1 / (\lambda - \kappa)$ and $\Psi_o = \lambda - \kappa$.

# 4

# Model performance and numerical validation

## 4.1 Model Performance

The constitutive behaviour of NS is described in this section through a series of material point analyses aimed to further illustrate the elasto-plastic characteristics of the presented model. For this purpose, the set of parameters reported in Table 3 (on page 20) is used for these computations. Although these parameters are not calibrated to fit a particular soil, they are selected within the range of values typical for sand-like materials which have been proposed in Jefferies and Been (2016) (on page 35) and reported in Table 2 (on page 19).

**Table 3: Model parameters employed in the material point computations presented in Figures. 8-13**

| $G_{ref}/p_{ref}$ | $p_{ref}$ [kPa] | $n_G$ | $\nu$ | $\Gamma$ | $\lambda_e$ | $M_{tc}$ | $N$ | $\chi_{tc}$ | $H_0$ | $H_\psi$ | R | S | $\psi_o$ |
|---|---|---|---|---|---|---|---|---|---|---|---|---|---|
| 350 | 100 | 0.5 | 0.2 | 1 | 0.03 | 1.2 | 0.35 | 4 | 300 | 0 | 1 | 0 | -0.15 |

The constitutive performance of the model is detailed in Figure 8 (on page 21) in which a drained triaxial compression test is computed for a dense sand ($\Psi_o$=*-0.15*) and for a given confining pressure equal to $p_o$=*200* kPa. In this figure, the stress path and the corresponding yield surface are plotted in combination with the hardening variables (i.e., the image stress $p_{im}$ and its maximum value $p_{max}$, Figure 8 (on page 21)) thus showing their evolution throughout the loading path. To further emphasize the effect of limiting dilatancy through a limit hardening, $p_{im}$ and $p_{max}$ are also plotted in Figure 8 (on page 21) with the difference $p_{max}$ - $p_{im}$ characterizing the incremental hardening reported in Eq. [4]. It is shown that the vanishing of this difference corresponds to the peak of the stress-strain response (Figure 8 (on page 21)) and mark the beginning of the post-peak behavior of the material. It is worth remarking that, at large strain, the material reaches the critical state (i.e., the intersection between the stress path and the CSL marked in Figure 8 (on page 21) as $q_{cs}$) and, as a result, the variables $\Psi$ and $\Psi_i$ (Figure 8 (on page 21)) tend to zero while the image stress $p_{im}$ tends to the mean effective stress at critical state. For the sake of clarity, the same test is repeated in Figure 9 (on page 21) by enforcing *50%* of axial strain, thus better highlighting the material behavior at critical state when loaded at large strain.

To further show the model performance, a set of drained and undrained triaxial tests performed at different confining pressure is plotted in Figure 10 (on page 22)-Figure 11 (on page 22) for both dense and loose states (i.e., for two values of the state parameter, $\Psi_o$=*0.15* and $\Psi_o$=*-0.15*, respectively) which emphasize the ability of the model to simulate liquefaction failure resulting from the excess pore-pressure in undrained stress paths and the capability to dilate and compact along drained triaxial compressions. Similarly, the ability of the model to simulate the mechanical response of a soil at different initial density is illustrate in Figure 12 (on page

23) and Figure 13 (on page 23) where a sensitivity analysis is proposed by varying the initial value of the state parameter.

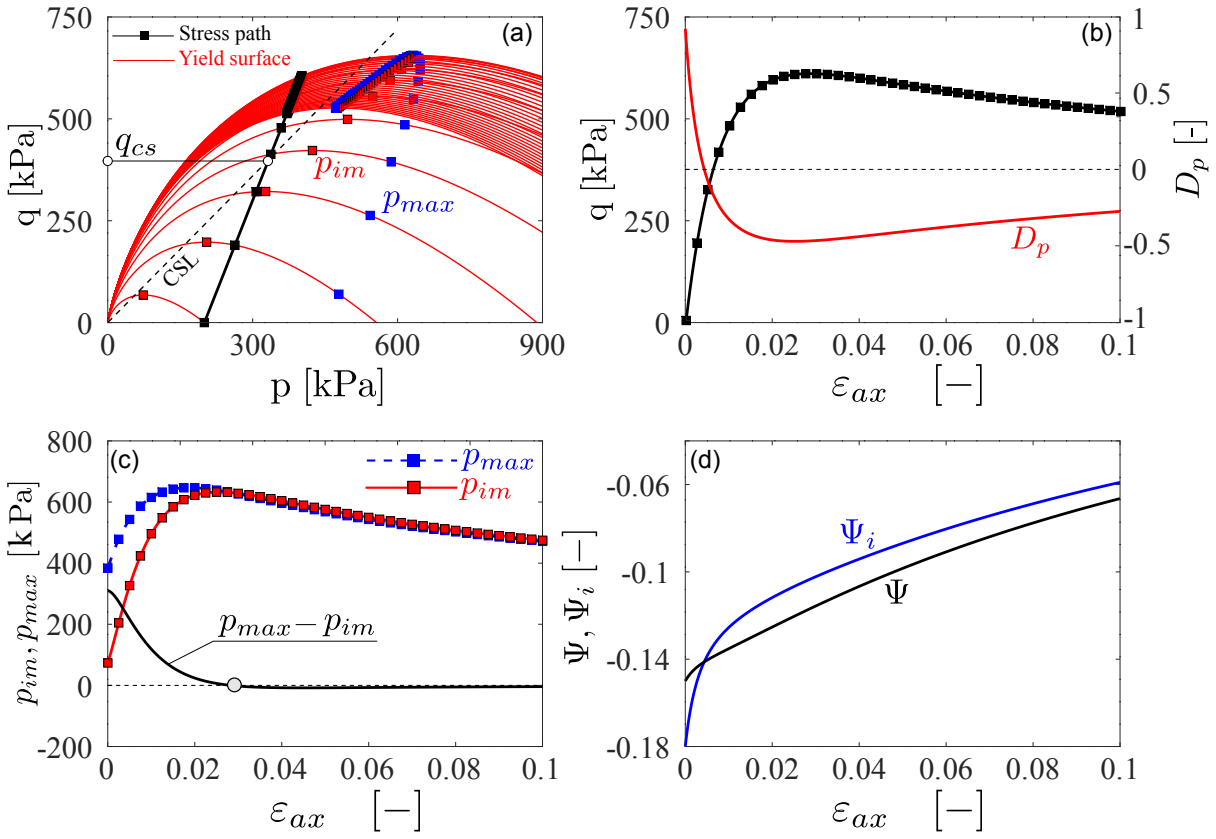


*Figure 8: Model response during a drained triaxial test characterized by an initial confining pressure equal to $p_o$=200 kPa for a dense sand (i.e., $\Psi_o$=-0.15)*

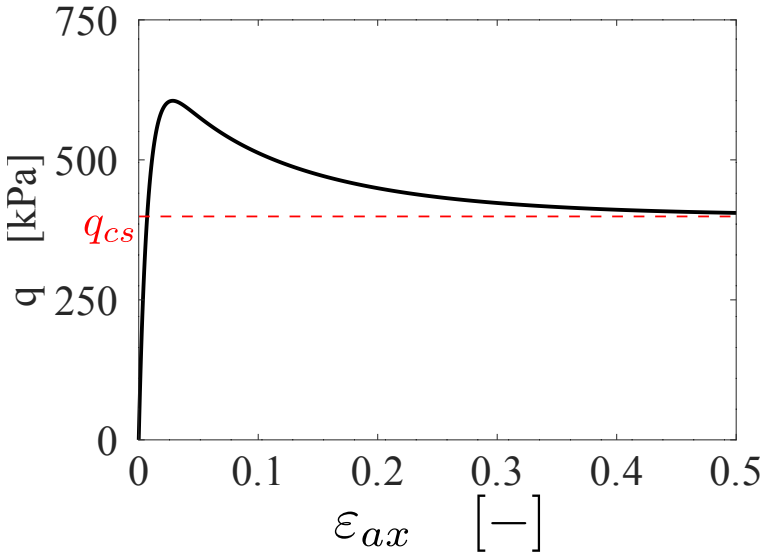


*Figure 9: Drained triaxial test plotted in Figure 8 loaded up to 50% of axial strain*

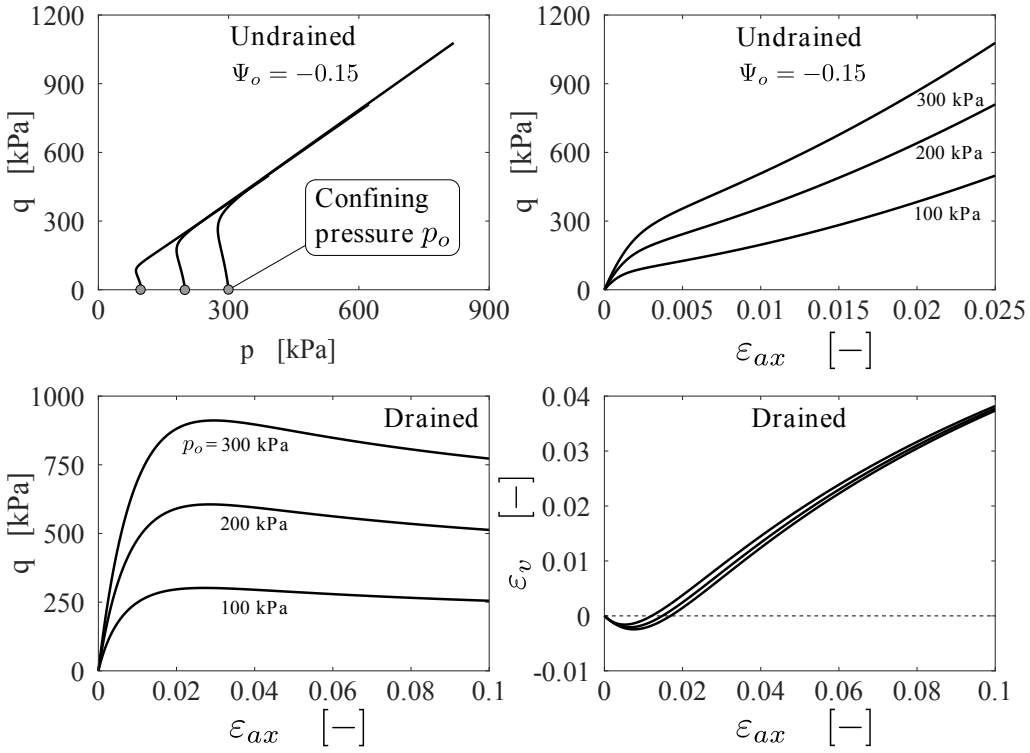


*Figure 10: Constitutive behaviour of NS model in dense conditions at different confining pressures*

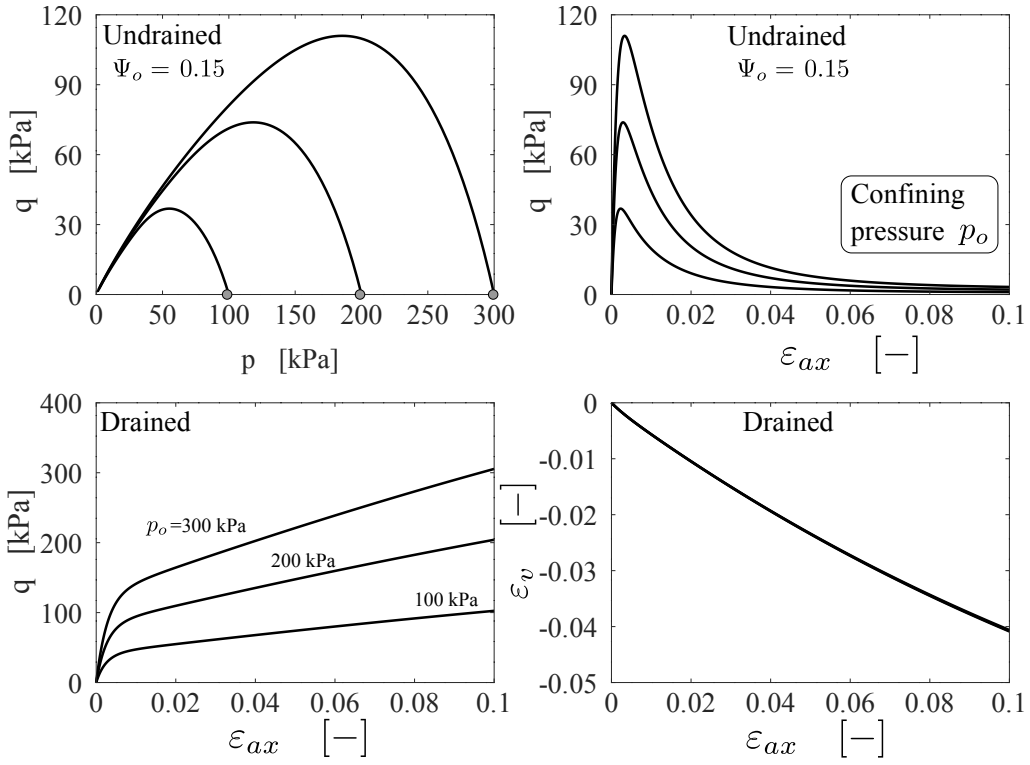


*Figure 11: Constitutive behaviour of NS model in loose conditions at different confining pressures*

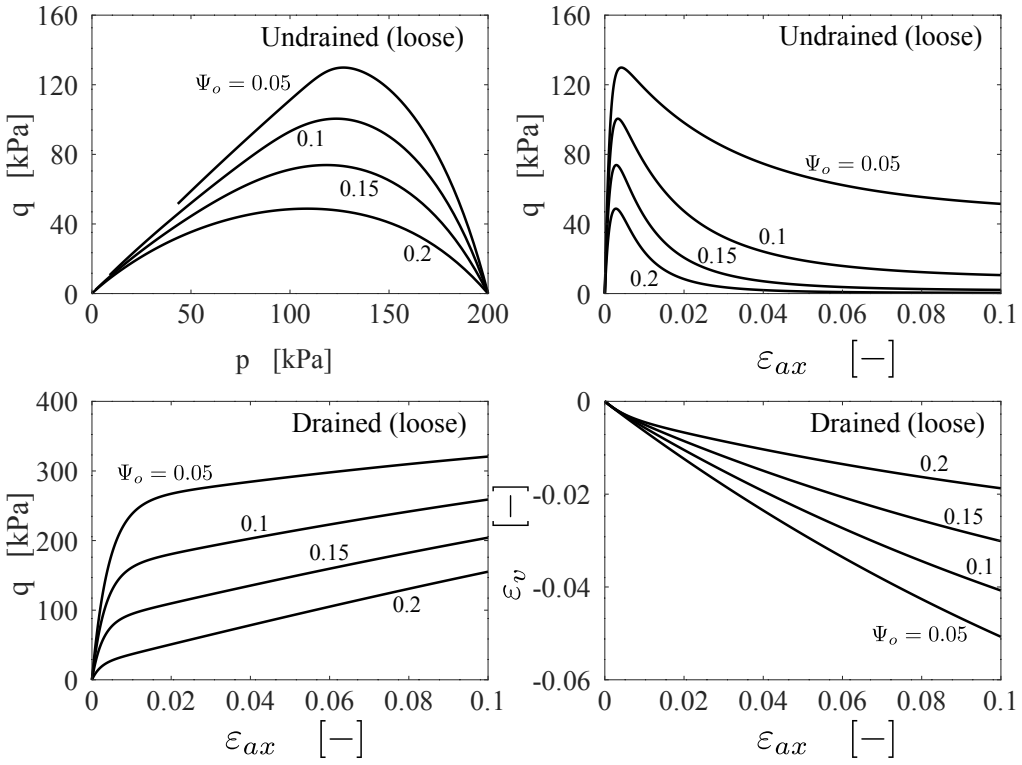


*Figure 12: Constitutive behaviour of NS model in loose conditions for different values of $\Psi_o$*

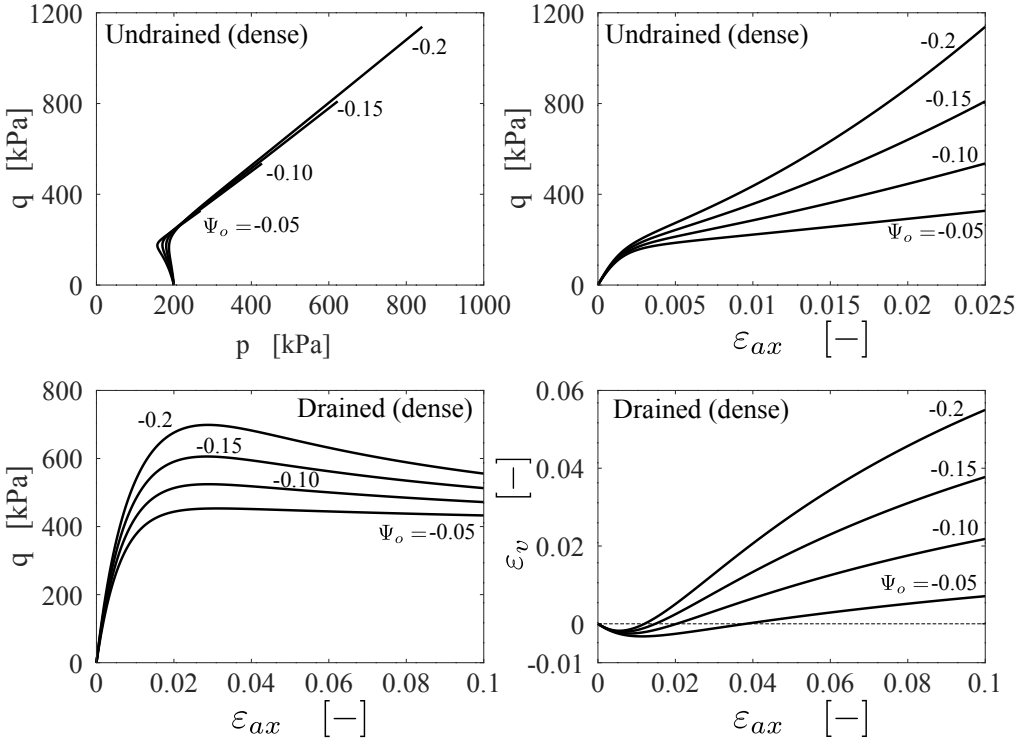


*Figure 13: Constitutive behaviour of NS model in dense conditions for different values of $\Psi_o$*

## 4.2 Numerical validation

To validate the numerical implementation of NS in PLAXIS Finite element, a series of material point analyses have been performed to compare the model behavior with the results obtained through a Visual Basic for Applications (i.e., VBA) spreadsheet in which a fully explicit algorithm (i.e., a Step Forward Euler method) is considered to integrate different stress paths. Provided by the authors of the model, the VBA script is here used to compute triaxial stress-paths for both drained and undrained conditions (i.e. TXD and TXU), as well as undrained direct simple shear tests (i.e., UDSS). As NS is implemented in PLAXIS to cope with more general stress-strain conditions, the comparison of the constitutive response obtained by using the two integration strategies can be used to validate the current implementation of the model. This comparison is shown in Figure 14 (on page 25) where the triaxial tests for both loose and dense conditions are computed with the parameters reported in Table 4 (on page 24). A similar result is also shown in Figure 15 (on page 25) where an undrained direct simple shear test is computed by considering both responses resulting from the activation of the softening flag (i.e., S = 0 and S = 1). Similar material point tests have been performed by using the power-law CSL (Eq. [4]) which parameters are reported in Table 5 (on page 24).

**Table 4: List of parameters used for the numerical validation of NS Model**

| $G_{ref}/p_{ref}$ | $p_{ref}$ [kPa] | $n_G$ | $\nu$ | $\Gamma$ | $\lambda_e$ | $M_{tc}$ | $N$ | $\chi_{tc}$ | $H_0$ | $H_\psi$ | R | S |
|---|---|---|---|---|---|---|---|---|---|---|---|---|
| 200 | 100 | 0.6 | 0.1 | 1.115 | 0.076 | 1.4 | 0.3 | 2.5 | 30 | 200 | 1 | 1 |

**Table 5: List of parameters used for the numerical validation of NS Model**

| $G_{ref}/p_{ref}$ | $p_{ref}$ [kPa] | $n_G$ | $\nu$ | $C_a$ | $C_b$ | $C_c$ | $M_{tc}$ | $N$ | $\chi_{tc}$ | $H_0$ | $H_\psi$ | R | S |
|---|---|---|---|---|---|---|---|---|---|---|---|---|---|
| 200 | 100 | 0.5 | 0.15 | 0.90 | 0.14 | 0.15 | 1.28 | 0.3 | 4.6 | 100 | 625 | 1.2 | 1 |

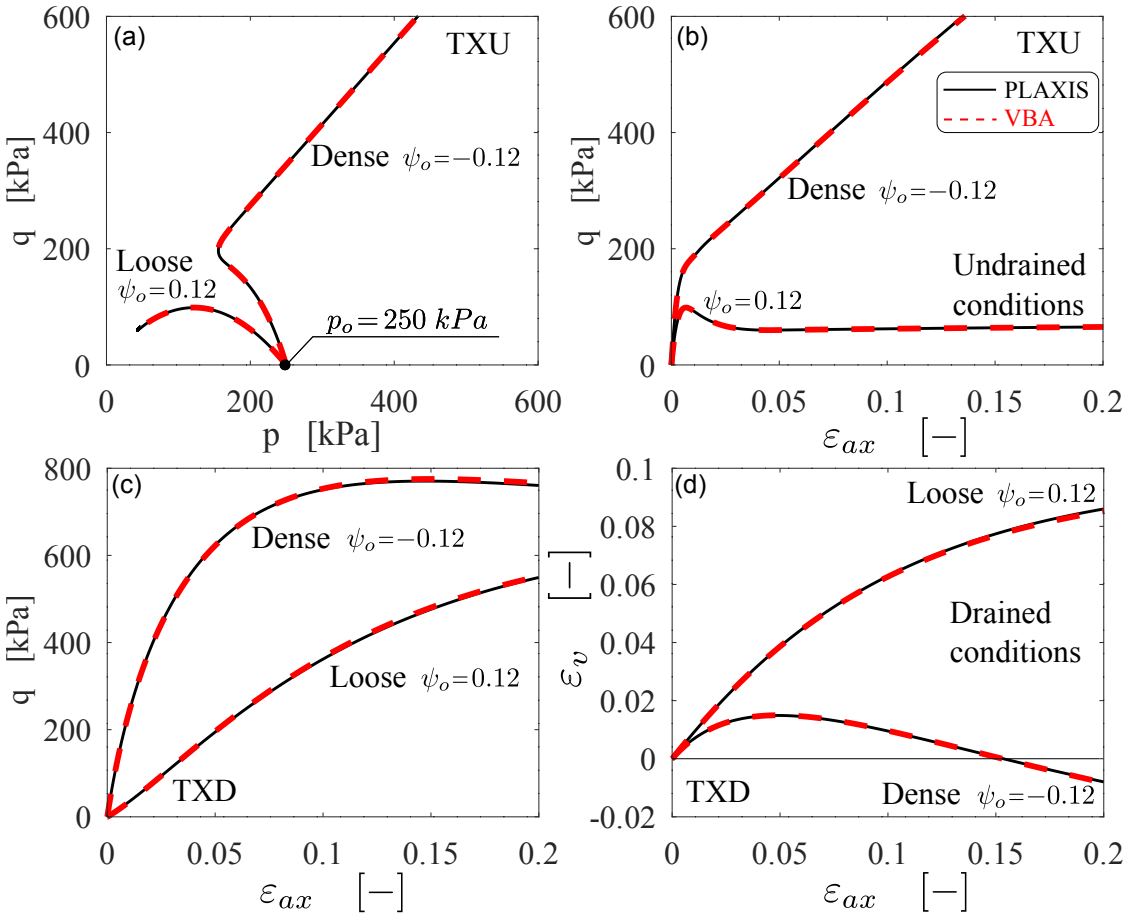


*Figure 14: Constitutive response resulting from drained and undrained triaxial tests: comparison between PLAXIS and VBA script.*

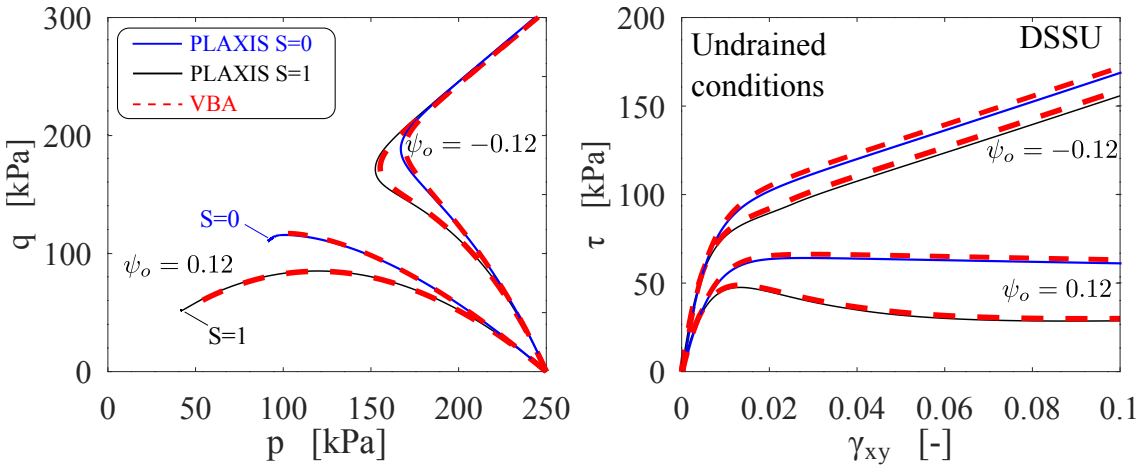


*Figure 15: Constitutive response resulting from undrained direct simple shear test: comparison between PLAXIS and VBA script.*

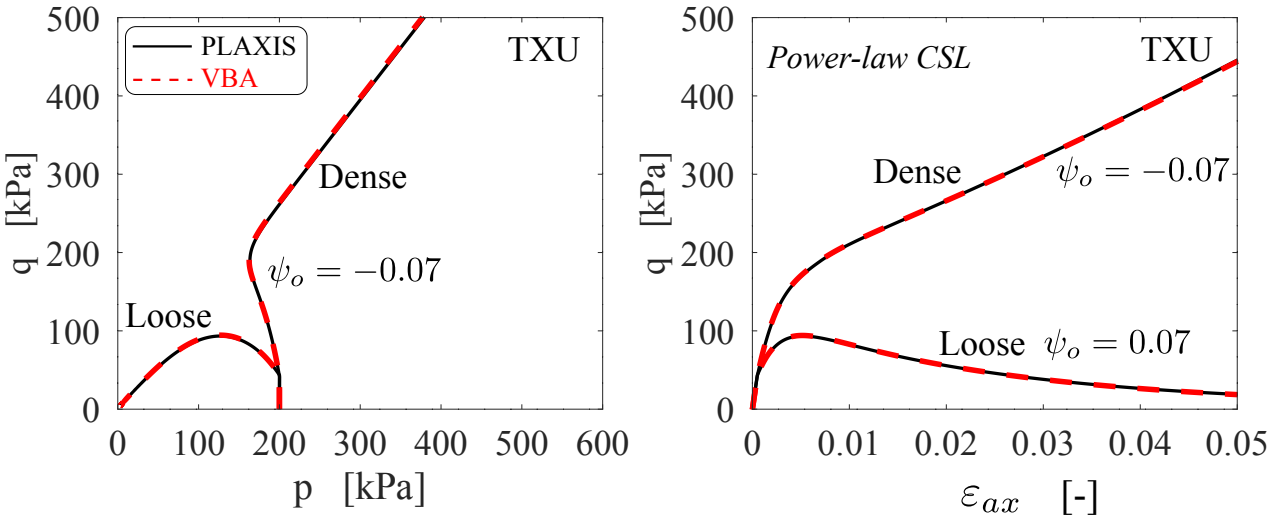


*Figure 16: Constitutive response resulting from undrained triaxial tests and a power-law CSL: comparison between PLAXIS and VBA script.*

# 5 UDSM implementation in PLAXIS finite element code

## 5.1 Material Parameters

NS model has been implemented as a User Defined Soil Model (UDSM) in PLAXIS finite element. The CSLs reported in Eq. [3] (i.e., the logarithmic and power-law formulations) are implemented in the same UDSM (i.e., the same DLL file called norsand.dll), and one of the two options can be selected in "Model in DLL": *i)* NorSand-CSL(a) to use the logarithmic expression of the CSL characterized by the parameters $\Gamma$ and $\lambda_e$ (Figure 17 (on page 27) ) or *ii)* NorSand-CSL(b) for the power-law CSL defined with the parameters $C_a$, $C_b$ and $C_c$ (Figure 17 (on page 27) ).

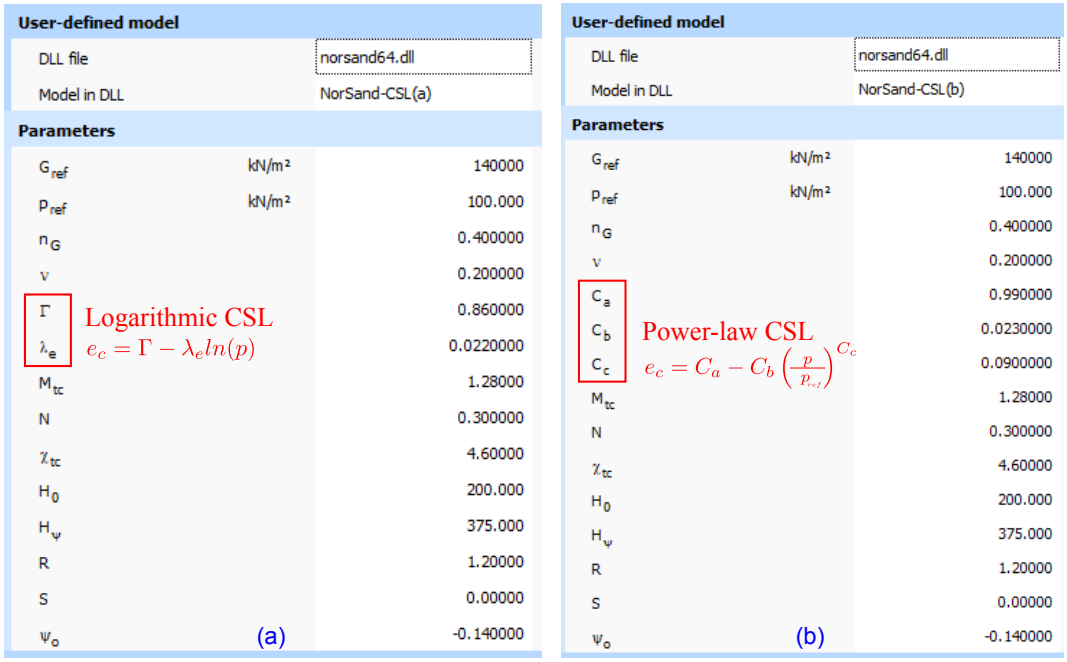


*Figure 17: Model parameters for both CSL formulations: (a) Logaritmic CSL, (b) Power-law CSL*

The parameters reported in Figure 17 (on page 27) are listed as follows:

$G_{ref}$ Reference value of the shear modulus at the reference pressure.

$p_{ref}$ Reference mean pressure (generally the common value of 100 kPa is used).

$n_G$ Exponent of the power-law elasticity.

$\nu$ Poisson's ratio.

$M_{tc}$ Friction ratio at critical state in triaxial conditions.

$N$ Material parameter controlling the maximum stress ratio as a function of the minimum dilatancy.

$\chi_{tc}$ Material parameter which governs the slope of the minimum dilatancy as a function of the state parameter.

$H_0$ Hardening parameter.

$H_\Psi$ Hardening parameter.

$R$ Over-consolidation ratio.

$\Psi_o$ Initial value of the state parameter.

The two formulations of the CSL are characterized by the following parameters:

- Logarithmic expression of the CSL (equation Eq. [3], option a).

  $\Gamma$ Void ratio corresponding to a mean pressure equal to 1 kPa.

  $\lambda_e$ Slope of the critical state ($e$-$ln(p)$).

- Power-law expression of the CSL (equation Eq. [3], option b).

  $C_a$ Void ratio corresponding to a mean pressure equal to 0 kPa.

  $C_b$ Parameter of the power-law expression.

  $C_c$ Exponent of the power-law.

The parameter $M_{tc}$ is here used for two purposes:

- To use the sign of $M_{tc}$ in order to switch between *Extended Dafalias* or *Modified Bishop*. If $M_{tc}>0$ (e.g., $M_{tc}$=1.2) as *Extended Dafalias* is considered, while the same value with opposite sign automatically selects the *Modified Bishop* expression (e.g., $M_{tc}$=-1.2). It is worth remarking that the two formulations are equivalent in case of dense soils (i.e., $\Psi_o<0$) while they result to modify the soil behavior in case of loose soils.
- To assign the value of the parameter $M_{tc}$ (i.e., $M_{tc}=|M_{tc}|$).

The parameter $S$ is used as a flag therefore only 0/1 can be selected. When a different value is prescribed, $S$ is automatically set to zero. Similarly, this flag is constrained to be used only in undrained conditions, therefore its effect is not taken into account in drained conditions.

## 5.2 State variables

To better visualize the results obtained from a finite element simulation, a set of state variables can be plotted by selecting in PLAXIS Output the option *User-defined parameters* (i.e., from **Stress** > **Stress State parameters** > **User-defined parameters**, Figure 18 (on page 29)). Here below the entire list of variables:

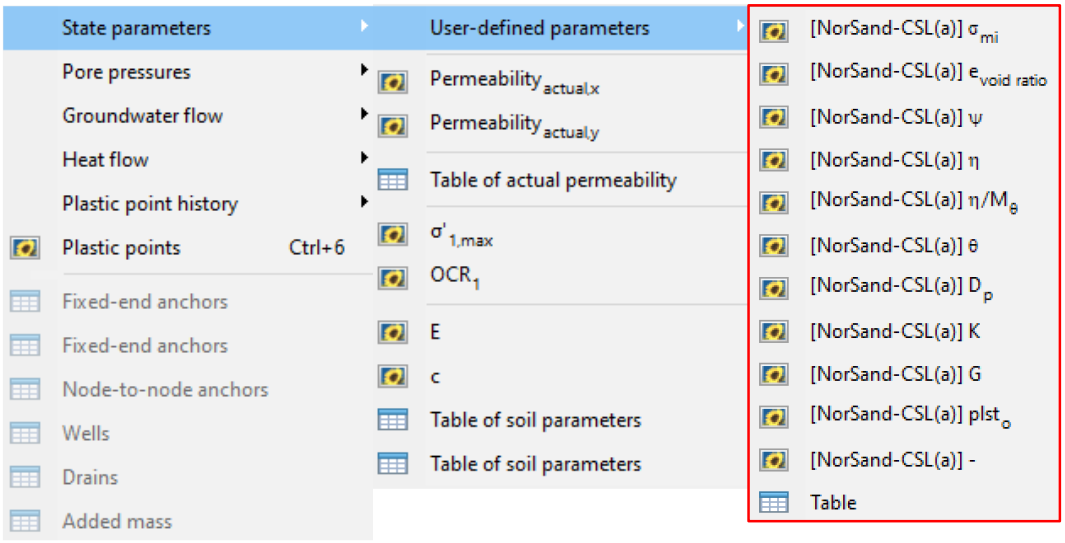


*Figure 18: List of User-defined paarmeters which can be ploted in PLAXIS output*

where

| | | |
|---|---|---|
| $\sigma_{mi}$ | = | The image stress is the hardening variable of the model. |
| $e_{void\ ratio}$ | = | Current void ratio of the model. |
| $\Psi$ | = | State parameters. |
| $\eta$ | = | Stress ratio. |
| $\eta/M_\theta$ | = | Stress ratio normalized with Eq. [7] |
| $\theta$ | = | Lode's angle. |
| $D_p$ | = | Dilatancy function. |
| $K$ | = | Bulk modulus. |
| $G$ | = | Shear modulus. |
| *plast* | = | Plastic points. |
| - | = | Used for internal purposes. |

It is worth remarking that, at the beginning of a given calculation phase, the value of the void ratio stored in *User-defined parameters* is initialized by inverting Eq. [3] where $\Psi$ is equal to the initial value of the state parameter (i.e., the $\Psi_0$ prescribed by the user), and the mean pressure results from the initial stress state. The advantage of this strategy is that the void ratio $e_{void\ ratio}$ is automatically re-scaled with the soil depth, thus avoiding subdividing the soil cluster in layers each characterized by a different value of the initial void ratio. For this reason, it is normal to observe different values between this variable (i.e., $e_{void}$ ratio from *State parameters*) and the void ratio reported in PLAXIS Output through the tab **Deformation** > **Total strain** which initial value is set in PLAXIS Input through the tab dedicated to material models (i.e., **General** > **Advanced** > $e_{init}$). At variance

with $e_{void}$ ratio, the value of $e_{init}$ is kept constant for all the points characterizing the initial state of a given cluster associated to a given material.

It is important to observe that, as many other constitutive frameworks, NS is a model which mobilizes the material strength through the evolution of the hardening variable $\sigma_{mi}$, for this reason it is not possible to use NS within the Strength Reduction Factor (SRF) method where the strength reduction is performed by a decrease of material parameter.

# 6 Finite Element Analyses

To show the performance of the implemented model to capture the liquefaction potential of loose sediments, an initial boundary value problem simulating a slope failure is computed with PLAXIS 2D and is presented in this section. The initial and boundary conditions are similar to the problem presented in Jefferies and Been (2016) and they are depicted in Figure 19 (on page 32). The loading process is aimed to simulate a flow liquefaction process which is triggered by applying a displacement of *20 cm* on the top of the slope through a rigid slab with the soil parameters representing a quartz sand with trace of silts (see Table 6 (on page 31)). To simulate flow liquefaction, undrained conditions are prescribed to the entire finite element domain.

The initialization of the stress state is performed through three different phases:

- An initial phase performed with calculation type $k_0$ *initialization* in which the formula of Jacky is used to calculate $k_0$. The value of $k_0 = 1 - sin(\phi) = 0.5$ is used in this example and corresponds to a friction angle $\phi = 30\ ^\circ$ selected to have a value close to the one obtained from the stress ratio at critical state (i.e., $sin(\phi) = 3M_{tc} / (6 + M_{tc})$).
- A plastic loading phase with no loading aimed to have an initial stress state in equilibrium with the soil weight according NS behaviour.
- A plastic loading phase in which the loading is applied until the soil reaches a failure state. In this phase, a reset of the state variables is checked in the numerical inputs to guarantee a correct calculation of the state variable with a previous stress state.

**Table 6: Model parameters proposed in Jefferies and Been (2016) to solve the slope failure problem presented in Figure 19**

| $G_{ref}/p_{ref}$ | $p_{ref}$ [kPa] | $n_G$ | $\nu$ | $\Gamma$ | $\lambda_e$ | $M_{tc}$ | $N$ | $\chi_{tc}$ | $H_0$ | $H_\psi$ | R | S |
|---|---|---|---|---|---|---|---|---|---|---|---|---|
| 300 | 100 | 1.0 | 0.15 | 0.875 | 0.03 | 1.27 | 0.35 | 4 | 100 | 0 | 1 | 0 |

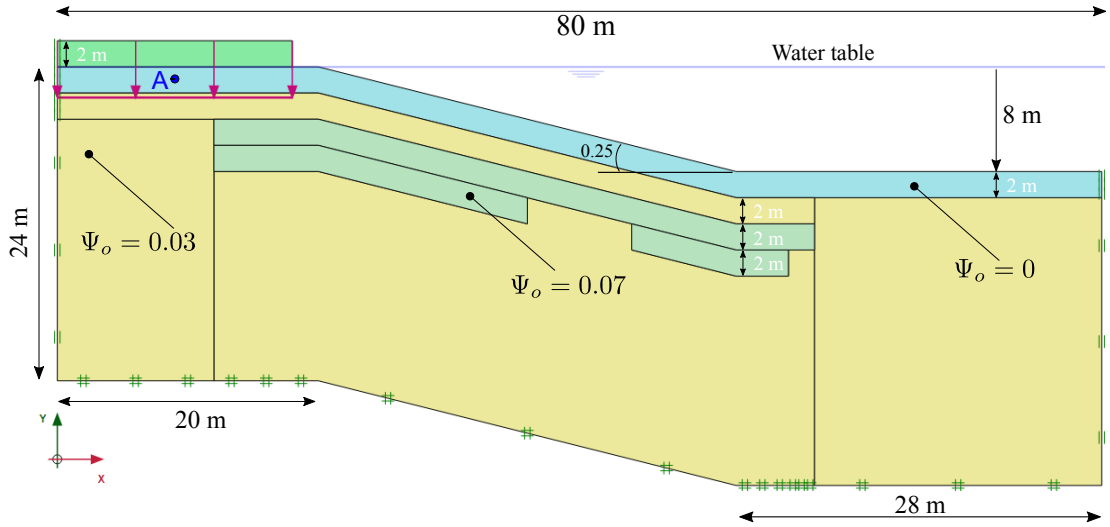


*Figure 19: Initial and boundary conditions of the finite element problem solved with PLAXIS 2D*

The results of the computed problem are shown in Figure 20 (on page 33) where the state of the soil at the end of the loading is characterized by the stress points in plastic loading (Figure 20 (on page 33)), the norm of cumulated displacements (Figure 20 (on page 33)) and the normalized stress ratio (Figure 20 (on page 33)). Figure 20 (on page 33) shows the region below the foundation undergoing through failure and enables to identify the undrained shear bands characterizing the failure process at the end of the loading. The mechanism of failure can be observed also in Figure 20 (on page 33) where the normalized stress ratio is plotted to quantify the residual frictional capabilities before reaching the critical stress ratio (i.e., when $\eta/M_\theta \approx 1$ the material reaches the critical state). It is shown that the stress points below the foundation are characterized by higher values of the normalized stress ratio ($\eta/M_\theta \approx 0.94$) which tends to decrease in zones of the soils farther from the foundation.

To differentiate the plastic points according to the hardening process, the existing symbols used in PLAXIS Output are employed with a different meaning:

- Failure points (*red square* □): plastic points at critical state.
- Hardening points (*downward green triangle* ▽ ): plastic points.
- Liquefaction points (*downward purple triangle* ▽ ): plastic points characterized by a stress ratio greater than the instability line.

it is worth nothing that liquefaction points are plotted also when the finite element analysis is performed in drained conditions thus highlighting potential liquefaction phenomena occurring if soil conditions switch from drained to undrained.

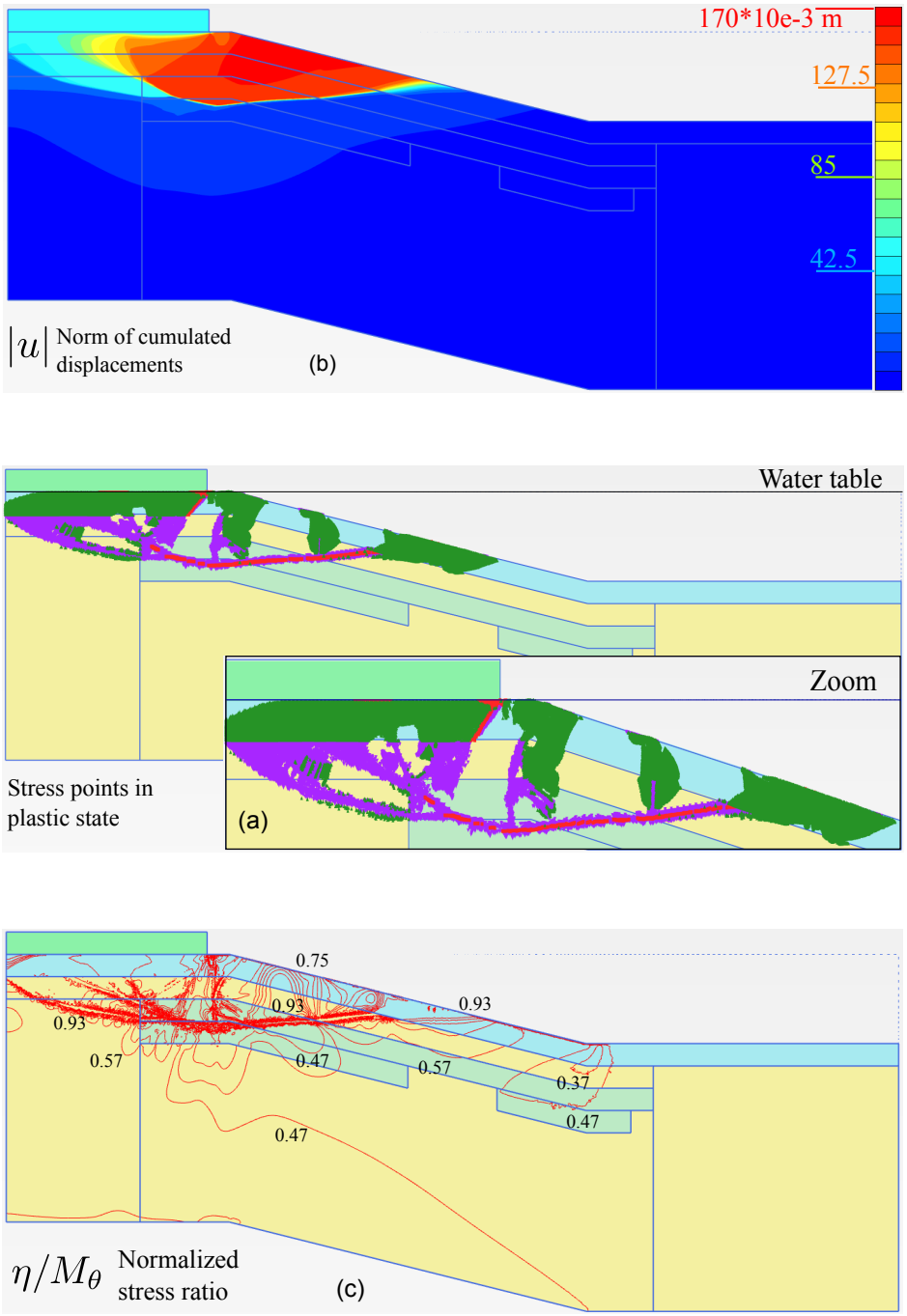


*Figure 20: Numerical solution of the finite element problem shown in Figure 17: (a) the distribution of Gauss point in plastic loading, (b) the norm of cumulated displacements, (c) normalized stress ratio.*

To further emphasize the effect of the initial porosity, the same computation has been solved with one single value of $\Psi_o$ for all the layers varying the value of the state parameter to simulate soils from dense to loose conditions (i.e., $\Psi_o$=0.0, $\Psi_o$=0.3, $\Psi_o$=0.5 and $\Psi_o$=0.7). The results are plotted in where the stress path of a stress point below the foundation (i.e., point A in Figure 19 (on page 32) ) is reported for the three different values of $\Psi_o$, thus highlighting the different trend of behaviour related to different initial void ratios.

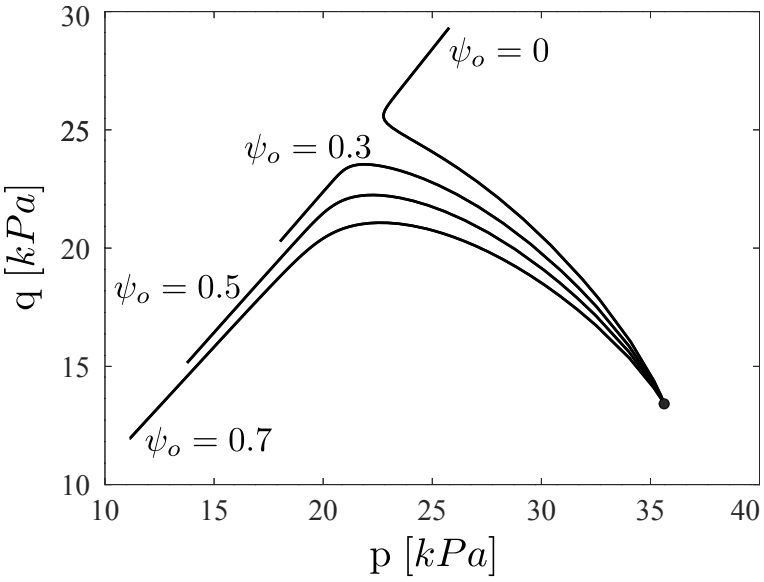


*Figure 21: Stress paths of the stress point below the foundation (i.e., point A reported in Figure 16) corresponding to different values of the state parameter (i.e., $\Psi_o$=0.0, $\Psi_o$=0.3, $\Psi_o$=0.5 and $\Psi_o$=0.7).*

**ACKNOWLEDGEMENTS**

Dr. Jefferies M. and Dr. Shuttle D. are gratefully acknowledged for their support, suggestions and time dedicated during the implementation of NS model.

# 7 References


1. Been, K., Jefferies, M. G., and Hachey, J. (1991). The critical state of sands. Géotechnique, 41(3):365-381.
2. Bishop, A. W. (1950). Reply to discussion on "measurement of shear strength of soils" by a.w. skemptonand and a.w. bishop. Géotechnique, 2:90-108.
3. Cho, G.-C., Dodds, J., and Santamarina, J. C. (2006). Particle shape effects on packing density, stiffness, and strength: Natural and crushed sands. *Journal of Geotechnical and Geoenvironmental Engineering*, 132(5).
4. Conforth, D. H. (1961). Plane strain failure characteristics of a saturated sand. PhD thesis, University of London.
5. Drucker, D. C. (1951). A more fundamental approach to stress-strain relations. In Proceedings of the First US National Congress of Applied Mechanics, pages 487-491. ASME, ASME.
6. Jefferies, M. (2020). On the fundamental nature of state parameter. Geotechnique. under review.
7. Jefferies, M. and Been, K. (2016). Soil Liquefaction, a Critical State Approach. Applied geotechnics series. CRC Press.
8. Jefferies, M. and Shuttle, D. (2011). On the operating critical friction ratio in general stress states. Géotechnique, 8(61):709-713.
9. Jefferies, M., Shuttle, D., and Been, K. (2015). Principal stress rotation as cause of cyclic mobility. Geotechnical Research, 2(2):66-96.
10. Li, X. S. and Dafalias, Y. F. (2000). Dilatancy for cohesionless soils. Géotechnicque, 50(4):449-460.
11. Lyman (1938). Construction of franklin falls dam. Technical report, US Army corps of engineers.
12. Resende, L. and Martin, J. B. (1985). Formulation of drucker& prager cap model. Journal of Engineering Mechanics, 111(7):855-881.
13. Schofield, A. N. and Wroth, C. P. (1968). Critical state soil mechanics. McGrow-Hill, London.